energies

MDPI

Article

A New State of Charge Estimation Algorithm for Lithium-Ion Batteries Based on the Fractional Unscented Kalman Filter

Yixing Chen [1], Deqing Huang [1,*], Qiao Zhu [2], Weiqun Liu [2], Congzhi Liu [3] and Neng Xiong [2]

[1] School of Electrical Engineering, Southwest Jiaotong University, Chengdu 610031, China; bk20110190@my.swjtu.edu.cn

[2] School of Mechanical Engineering, Southwest Jiaotong University, Chengdu 610031, China; zhuqiao@home.swjtu.edu.cn (Q.Z.); weiqunliu@home.swjtu.edu.cn (W.L.); swjtuxiongneng@163.com (N.X.)

[3] The State Key Laboratory of Automotive Safety and Energy, Tsinghua University, Beijing 100084, China; 15281063684@163.com

* Correspondence: elehd@home.swjtu.edu.cn; Tel.: +86-028-87601026

Received: 18 July 2017; Accepted: 26 August 2017; Published: 1 September 2017

Abstract: An accurate state of charge (SOC) estimation is the basis of the Battery Management System (BMS). In this paper, a new estimation method which considers fractional calculus is proposed to estimate the lithium battery state of charge. Firstly, a modified second-order RC model based on fractional calculus theory is developed to model the lithium battery characteristics. After that, a pulse characterization test is implemented to obtain the battery terminal voltage and current, in which the parameter identification is completed based on least square method. Furthermore, the proposed method based on Fractional Unscented Kalman Filter (FUKF) algorithm is applied to estimate the battery state of charge value in both static and dynamic battery discharging experiment. The experimental results have demonstrated that the proposed method shows high accuracy and efficiency for state of charge estimation and the fractional calculus contributes to the battery state of charge estimation.

Keywords: second-order RC circuit model; fractional calculus; Fractional Unscented Kalman Filter; SOC estimation

1. Introduction

In response to the concerns of the energy depleting and environment protection, electric vehicles and hybrid electric vehicles are proposed as popular substitutions for conventional fossil fuel vehicles for a wide range [1]. Battery Management System (BMS) is one of the core technologies of electric vehicles. An advanced BMS can avoid the potential safety hazard and ensure efficient operation as well [2]. State of charge (SOC) estimation performs as a significant factor of BMS performance, which is defined as the percentage of the left battery coulomb to the rated capacity and SOC cannot be measured directly [3], thus, SOC estimation is usually achieved by the measurable battery terminal voltage and the battery current.

The accurate state estimation with the terminal voltage and the current is a complicated issue [4], because the battery is a strong non-linear system within the charge and discharge process [5]. In recent years, many scholars have proposed substantial methods to improve the accuracy of SOC estimation, such as Ampere hour counting [6], Kalman Filter (KF) [7], $H\infty$ observer [8], sliding model observer [9], etc. Ampere hour counting is an extensively utilized method, which applies integrals with respect to the battery current, but it heavily depends on the accuracy of the current measurement and the initial *SOC* value [10]. The errors of current measurement and initial *SOC* value can cause the accumulation of the SOC estimation error, which cannot be corrected. KF is another widely used method to estimate

SOC, which sets recursive equations to minimize the state error [11]. KF is not sensitive to the noise because it considers the mean and covariance of the process noise and measurement noise [12]. Plett adopted Extended Kalman Filter (EKF) on SOC estimation of Li-ion battery [7]. The SOC estimation of the battery is a non-linear system problem [13]. EKF linearizes the non-linear battery model with Taylor expansion. Usually only the first order term of Taylor expansion is used to avert the mass calculation, thus this causes the accumulation of the state error in the process of iteration and the derivation of the Jacobian matrices [14]. Unscented Kalman Filter (UKF) has also been investigated for non-linear system [15,16]. Compared with EKF, UKF with Unscented Transformation (UT) doesn't contain the linearization of the system and it provides a series of carefully chosen sigma points [13], which offers better covariance approximation and higher precision than EKF due to its at least second order approximation items of nonlinear system [17]. D'Alfonso et al. have utilized UKF in mobile robot localization problem [18]. Miyabayashi et al. have adopted UKF on state estimation of tubular microreactors [19]. He et al. have used UKF in battery SOC estimation [20]. All of their papers demonstrate that UKF shows higher precision than EKF in different real systems.

In recent years, many scholars, such as Monje, found that non-linear systems have fractional properties [21]. Fractional calculus, which is an expansion of the integer calculus, depicts the non-integer order integration and derivative, and fractional calculus describes the memorial and hereditary properties of systems [22]. Ortigueira and Machado point out that fractional models can describe dynamical behaviour of the systems and they exhibit better capability of fitting experimental data [23]. Thus, fractional calculus is widely used in non-linear systems, including signal processing [24], as well as SOC estimation. Zhang et al. established a fractional-order model using a Walburg-like ultracapacitors, and adopted fractional Kalman filter to estimate the battery SOC [25]. Liu et al. established a fractional-order PNGV model and Extended Fractional Kalman Filter (EFKF) to implement the state estimation [26]. These scholars have proved that fractional calculus is capable of accurately depicting system performance in real system. Thus, considering the advantages of UKF in contrast to KF and EKF in integer systems mentioned above, it is reasonable and practicable to combine fractional calculus with UKF to propose a new method, which may be useful for battery SOC estimation accuracy. Therefore, the main contributions of this paper are: (1) developing an equivalent second-order resistance-capacitance (RC) circuit model with fractional operator; (2) developing a UKF algorithm combined with fractional calculus to estimate the battery SOC. The combination of fractional calculus and UKF takes full advantages of the merits of them. The new proposed algorithm contains more battery model parameters identified, and this helps the accuracy of SOC estimation. In addition, the proposed FUKF in this paper is also helpful for other filtering problem, which is meaningful for practical engineering application.

In this paper, a fractional second-order RC model is established in Section 2 and Fractional Unscented Kalman Filter (FUKF) is developed in Section 3. The procedure of parameter identification for the fractional model is given in Section 4. The results in Section 5 confirm that FUKF is advantageous to SOC estimation.

2. Battery Modeling

SOC estimation is one of the most important issues of an electrical vehicle BMS, and the foundation of precise SOC estimation is an accurate battery model. The first-order RC model, the simple model etc. are extensively used in battery SOC estimation [27]. The second-order RC model is utilized in this paper because it provides an accurate approximation for Li-ion battery dynamics [28].

2.1. Integer Second-Order RC Model

The model contains two capacitors, which are also suitable for the use of fractional calculus. Meanwhile, because of the model's simplicity and universality, this model is adopted as equivalent circuit model in this paper. The structure of second-order RC model is shown as Figure 1. In Figure 1, E represents the ideal battery electrodynamic force. The battery inner resistor R_0 accounts for the

resistance between the battery plate, electrolyte and electrodes. R_1 and C_1 describe the resistance and capacitance of the activation polarization effect, respectively. R_2 and C_2 depict the resistance and capacitance of the battery concentration polarization effect, respectively. All parameters are nonlinear functions of SOC value.

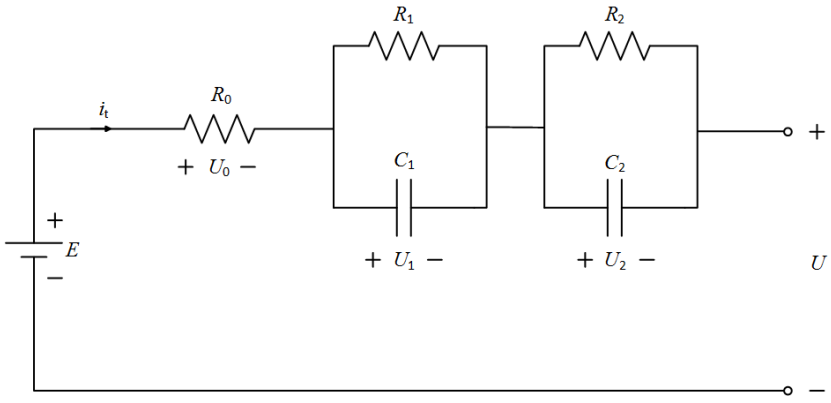

Figure 1. The circuit of the second-order RC model.

The state-space equation of the second-order RC model is:

$$\begin{aligned} \begin{bmatrix} \dot{U}_1 \\ \dot{U}_2 \end{bmatrix} &= \begin{bmatrix} -\frac{1}{R_1C_1} & 0 \\ 0 & -\frac{1}{R_2C_2} \end{bmatrix} \begin{bmatrix} U_1 \\ U_2 \end{bmatrix} + \begin{bmatrix} \frac{1}{C_1} \\ \frac{1}{C_2} \end{bmatrix} I(t) \\ U &= \begin{bmatrix} -1 & -1 \end{bmatrix} \begin{bmatrix} U_1 \\ U_2 \end{bmatrix} - I(t)R_0 + E \end{aligned} \tag{1}$$

where I and U are the battery current and the terminal voltage, respectively. U_0 is the voltage of R_0. U_1 and U_2 are the voltages of the two RC loops, respectively.

2.2. The Definition of Fractional Capacitor

Westerlund and Ekstam pointed out that the majority of capacitors shows fractional characteristics in practical dynamic conditions [29]. A fractional capacitor model, which is formed in frequency domain, is established to represent the fractional properties of the capacitors. The definition of the fractional capacitor is given as:

$$Z(j\omega) = \frac{1}{C_f(j\omega)^n}, 0 < n < 1 \tag{2}$$

where C_f is the capacitance of the capacitor, and n is the fractional order of the fractional capacitor.

2.3. The Definition and Properties of Fractional-Order Calculus

The fractional order Grünwald-Letnikov calculus formulation is given by the following equation [26]:

$$D_t^\alpha f(t) = \lim_{h \to 0} h^{-\alpha} \sum_{j=0}^{L} w_j^\alpha f(t - jh) \tag{3}$$

where D_t^α represents the fractional calculus operator with respect to the variable t; α is the order of the system; h is the sampling interval time; L is memory or window length. The factor $w_j^\alpha = (-1)^j \binom{\alpha}{j}$, and $\binom{\alpha}{j}$ is Newton binomial coefficient, thus this derives $w_0^\alpha = 1; w_j^\alpha = (1 - \frac{\alpha+1}{j}) w_{j-1}^\alpha, j = 1, 2, ..., k$.

In Equation (3), the value of α determines the type of the function. When $\alpha > 0$, the function is differential. When $\alpha = 0$, the function is the original function. When $\alpha < 0$, the function is integral. The formula is shown as the followings:

$$D_t^\alpha f(t) = \begin{cases} \dfrac{d^\alpha}{dt^\alpha} f(t) = \lim\limits_{h \to 0} h^{-\alpha} \sum\limits_{j=0}^{k} w_j^\alpha f(t - jh) & \alpha > 0 \\ f(t) & \alpha = 0 \\ \int_0^t f(\tau)(d\tau)^{-\alpha} = \lim\limits_{h \to 0} h^\alpha \sum\limits_{j=0}^{k} w_j^{-\alpha} f(t - jh) & \alpha < 0 \end{cases} \tag{4}$$

2.4. Fractional Second-Order RC Model

According to the equivalent circuit shown as Figure 1, the fractional second-order RC model is established when the capacitors of the second-order RC model are replaced by the fractional order capacitors. Then the state-space equation is derived as the followings:

$$\begin{gathered} \begin{bmatrix} \frac{d^\alpha}{dt^\alpha} U_1 \\ \frac{d^\beta}{dt^\beta} U_2 \end{bmatrix} = \begin{bmatrix} -\frac{1}{R_1 C_1} & 0 \\ 0 & -\frac{1}{R_2 C_2} \end{bmatrix} \begin{bmatrix} U_1 \\ U_2 \end{bmatrix} + \begin{bmatrix} \frac{1}{C_1} \\ \frac{1}{C_2} \end{bmatrix} I(t) \\ U = \begin{bmatrix} -1 & -1 \end{bmatrix} \begin{bmatrix} U_1 \\ U_2 \end{bmatrix} - I(t) R_0 + E \end{gathered} \tag{5}$$

The widely used SOC estimation method is the Ah (amper/hour) counting method shown as the followings:

$$SOC(t) = SOC_0 + \frac{\int_0^t \eta i(t)}{Q_N} dt \tag{6}$$

where SOC_0 is the initial SOC value. Q_N is the rated battery capacity. η is the charge-discharge efficiency, which is related to the battery working temperature, charge and discharge rate etc. The value of η can be set into the range of 0.92 to 0.998 [30]. In this paper, it is set to 0.98 for the convenience of the calculation.

Equation (5) with Equation (6) are combined, and the discrete fractional second-order RC model is obtained as the followings:

$$\begin{aligned} x_k &= A_{k-1} x_{k-1} + B_{k-1} I_{k-1} + w_{k-1} - \sum_{j=1}^{k} K_j x_{k-j} \\ U_k &= C_k x_k - I_k R_0 + E + v_k \end{aligned} \tag{7}$$

where $A_{k-1} = diag\{-\frac{h^\alpha}{R_1 C_1}, -\frac{h^\beta}{R_2 C_2}, 1\}$, $B_{k-1} = [\frac{h^\alpha}{C_1}, \frac{h^\beta}{C_2}, -\frac{\eta_{k-1} h}{Q_N}]^T$, $C_k = [-1, -1, 0]$. The state vector $x_k = [U_1(k), U_2(k), SOC(k)]^T$, and the fractional order factor $K_j = diag\{w_j^\alpha, w_j^\beta, 0\}$. Theoretically, the entire past estimated states should be considered. However, this may cause the computation burden in real system, thus the past states are shortened to avoid the computation burden according to short memory principle proposed by Caponetto et al. [31]. E is the electromotive force of the battery. w_k and v_k are the system noise and measurement noise, respectively. They obey normal distribution and both of them are independent zero-mean Gauss white noise with covariance matrices Q_k and R_k, respectively. In Equation (7), all the parameters including R_0, R_1, R_2, C_1, C_2, E vary with the SOC value, thus, the model is nonlinear. FUKF is then proposed by applying UKF to this nonlinear fractional second-order RC model.

3. Fractional Unscented Kalman Filter

For fractional second-order RC model, normal integer UKF is not applicable, thus UKF needs to be modified to fit the fractional second-order RC model. FUKF is a method based on fractional calculus and UKF and it is specially proposed in this section for the fractional battery model, including fractional second-order RC model. The observability is discussed and the detail process of FUKF is presented in this section.

3.1. The Observability of the Battery Model

As Equation (7) shows, the battery *SOC* value is included in the state vector. This explains that the estimation of the battery *SOC* value equals the observation of the state vector, thus it is important to ensure the observability of the model before the SOC estimation. For the discrete-time model, the model is observable if for any initial state x_0 and some final time k_f the initial state x_0 can be uniquely determined by knowledge of the input I_k and output U_k for all $i \in [0, k_f]$ [32].

From Equation (7), the derivation is performed to separate x_0 out as the followings:

$$\begin{aligned}
x_1 &= (A_0 - K_1)x_0 + B_0 I_0 \\
U_1 &= C_1 A_0 x_0 + C_1 B_0 I_0 - R_0 I_1 + E_1 - C_1 K_1 x_0 \\
x_2 &= (A_1 - K_2)x_1 + B_1 I_1 \\
&= A_1 A_0 x_0 + A_1 B_0 I_0 + B_1 I_1 - A_1 K_1 x_0 - \sum_{j=1}^{2} K_j x_{2-j} \\
U_2 &= C_2(A_1 A_0 x_0 + A_1 B_0 I_0 + B_1 I_1) - R_0 I_2 + E_2 - C_2 A_1 K_1 x_0 - C_2 \sum_{j=1}^{2} K_j x_{2-j} \\
&\cdots \\
x_k &= A_{k-1} x_{k-1} + B_{k-1} I_{k-1} - \sum_{j=1}^{k} K_j x_{k-j} \\
&= \prod_{i=0}^{k-1} A_i x_0 + B_{k-1} I_{k-1} + \sum_{i=0}^{k-2} \Big(\prod_{j=i+1}^{k-1} A_j \Big) B_i I_i + G(x) \\
U_k &= C_k \prod_{i=0}^{k-1} A_i x_0 + C_k [B_{k-1} I_{k-1} + \sum_{i=0}^{k-2} \Big(\prod_{j=i+1}^{k-1} A_j \Big) B_i I_i] + R_0 I_k + E_k + C_k G_k
\end{aligned}$$

Thus, the nonlinear equation can be obtained as:

$$Y = M x_0 + F(I, E) + G(x) \tag{8}$$

where

$$Y = \begin{pmatrix} U_0 \\ U_1 \\ U_2 \\ \cdots \\ U_k \end{pmatrix}$$

$$M = \begin{pmatrix} C_0 \\ C_1 A_0 \\ C_2 A_1 A_0 \\ \cdots \\ C_k \Big(\prod_{i=0}^{k-1} A_i \Big) \end{pmatrix}$$

$$F(I,E) = \begin{pmatrix} R_0 I_0 + E_0 \\ C_1 B_0 I_0 + R_0 I_1 + E_1 \\ C_2(B_1 I_1 + A_1 B_0 I_0) + R_0 I_2 + E_2 \\ \cdots \\ C_k[B_{k-1} I_{k-1} + \sum_{i=0}^{k-2} (\prod_{j=i+1}^{k-1} A_j) B_i I_i + R_0 I_k + E_k \end{pmatrix}$$

Noticing that M is the linear part of the model, and $G(x)$ is the nonlinear part of the model. $M^T M$ is an invertible matrix, thus,

$$x_0 = (M^T M)^{-1} M^T [Y - F(I,E) - G(x)]$$

As Brouwer Fixed Point Theorem illustrates, every continuous function mapping the disk to itself has a fixed point [33], thus the nonlinear equation Equation (8) has a unique solution, which means the initial state x_0 can be uniquely determined. This demonstrates that the discrete-time model in Equation (7) is observable.

3.2. Details of Fractional Unscented Kalman Filter

FUKF is based on unscented transformation which approximates the probability distribution of the variable by using sigma points [34]. For convenience, the n-dimensional discrete fractional model in Equation (7) is rewritten as Equation (9).

$$\begin{aligned} x_k &= f(x_{k-1}, u_{k-1}) + w_{k-1} \\ y_k &= h(x_k, u_k) + v_k \end{aligned} \tag{9}$$

where u_k is the input of the model, which is equal to i_k in Equation (7). y_k is the output of the model, which is equal to U_k in Equation (7). and the process steps of FUKF are given as the followings:

Step 1: Initialize the state vector and the covariance matrix:

$$\begin{aligned} \hat{x}_0^+ &= E(x_0) \\ P_0^+ &= E[(x_0 - \hat{x}_0^+)(x_0 - \hat{x}_0^+)^T] \end{aligned} \tag{10}$$

Step 2: In FUKF, a series of sigma points are adopted to estimate the system mean and covariance matrix at time k according to the optimal mean and covariance estimation at time $k-1$. The number of the sigma points is $2n+1$, where n is the scaling parameter of the state vector.

$$\begin{aligned} \hat{x}_{k-1}^{(0)} &= \hat{x}_{k-1}^+ \\ \hat{x}_{k-1}^{(i)} &= \hat{x}_{k-1}^+ + (\sqrt{(n+\lambda)P_{k-1}^+})_i \qquad i = 1, ..., n \\ \hat{x}_{k-1}^{(i)} &= \hat{x}_{k-1}^+ - (\sqrt{(n+\lambda)P_{k-1}^+})_{i-n} \quad i = n+1, ..., 2n \end{aligned} \tag{11}$$

where $\lambda = a^2(n+\kappa)$, and a is the parameter that determines the distribution of the sigma points. The constant κ is generally set to $3-n$. $(\sqrt{(n+\lambda)P_{k-1}^+})_i$ is the ith column of the Cholesky decomposition of the matrix $(n+\lambda)P_{k-1}^+$ [35].

Step 3: Transform sigma points from time $k-1$ to time k:

$$\hat{x}_k^{(i)} = f(\hat{x}_{k-1}^{(i)}, u_k) \tag{12}$$

Step 4: Calculate the mean and the covariance matrix of the sigma points for the prior state estimation at time k and it needs optimal state variable $\hat{x}_1^+, ..., \hat{x}_{k-1}^+$:

$$\begin{aligned} \hat{x}_k^- =& E(x_k|\hat{x}_1^+, ..., \hat{x}_{k-1}^+) \\ =& E(f(\hat{x}_{k-1}^{(i)}, u_k) - \sum_{j=1}^{k} K_j \hat{x}_{k-j}^+) \\ =& \sum_{i=0}^{2n} W_i^{(m)} \hat{x}_k^{(i)} - \sum_{j=1}^{k} K_j \hat{x}_{k-j}^+ \end{aligned} \tag{13}$$

where the weights of the sigma points are given as the followings:

$$\begin{aligned} W_0^{(m)} &= \frac{\lambda}{n+\lambda} \\ W_0^{(c)} &= \frac{\lambda}{n+\lambda} + 1 - a^2 + b \\ W_i^{(m)} &= W_i^{(c)} = \frac{1}{2(n+\lambda)} \qquad i = 1, ..., 2n \end{aligned} \tag{14}$$

where b is set to 2, as the optimal value to incorporate the prior knowledge of Gauss distribution of the state vector [35]. In addition, the covariance matrix is:

$$\begin{aligned} P_k^- &= E((\hat{x}_k^{(i)} - \hat{x}_k^-)(\hat{x}_k^{(i)} - \hat{x}_k^-)^T) + Q_k \\ &= E((f(\hat{x}_{k-1}^{(i)}, u_k) - E(f(\hat{x}_{k-1}^{(i)}, u_k)) + \sum_{j=1}^{k} K_j \hat{x}_{k-j}^+) \cdot \\ &\quad (f(\hat{x}_{k-1}^{(i)}, u_k) - E(f(\hat{x}_{k-1}^{(i)}, u_k)) + \sum_{j=1}^{k} K_j \hat{x}_{k-j}^+)^T) + Q_k \\ &= E((f(\hat{x}_{k-1}^{(i)}, u_k) - E(f(\hat{x}_{k-1}^{(i)}, u_k)))(f(\hat{x}_{k-1}^{(i)}, u_k) - E(f(\hat{x}_{k-1}^{(i)}, u_k)))^T \\ &\quad + \sum_{j=1}^{k} K_j \hat{x}_{k-j}^+ (f(\hat{x}_{k-1}^{(i)}, u_k) - E(f(\hat{x}_{k-1}^{(i)}, u_k)))^T + (f(\hat{x}_{k-1}^{(i)}, u_k) \\ &\quad - E(f(\hat{x}_{k-1}^{(i)}, u_k)))(\sum_{j=1}^{k} K_j \hat{x}_{k-j}^+)^T + \sum_{j=1}^{k} K_j \hat{x}_{k-j}^+ (\hat{x}_{k-j}^+)^T (K_j)^T) + Q_k \\ &= E((f(\hat{x}_{k-1}^{(i)}, u_k) - E(f(\hat{x}_{k-1}^{(i)}, u_k)))(f(\hat{x}_{k-1}^{(i)}, u_k) - E(f(\hat{x}_{k-1}^{(i)}, u_k)))^T) \\ &\quad + \sum_{j=1}^{k} K_j \hat{x}_{k-j}^+ E((f(\hat{x}_{k-1}^{(i)}, u_k) - E(f(\hat{x}_{k-1}^{(i)}, u_k)))^T) + E(f(\hat{x}_{k-1}^{(i)}, u_k) \\ &\quad - E(f(\hat{x}_{k-1}^{(i)}, u_k)))(\sum_{j=1}^{k} K_j \hat{x}_{k-j}^+)^T + \sum_{j=1}^{k} K_j \hat{x}_{k-j}^+ (\hat{x}_{k-j}^+)^T (K_j)^T + Q_k \\ &= E((f(\hat{x}_{k-1}^{(i)}, u_k) - \sum_{i=0}^{2n} W_i^{(m)} \hat{x}_k^{(i)})(f(\hat{x}_{k-1}^{(i)}, u_k) - \sum_{i=0}^{2n} W_i^{(m)} \hat{x}_k^{(i)})^T) \\ &\quad + \sum_{j=1}^{k} K_j \hat{x}_{k-j}^+ E((f(\hat{x}_{k-1}^{(i)}, u_k) - \sum_{i=0}^{2n} W_i^{(m)} \hat{x}_k^{(i)})^T) + E(f(\hat{x}_{k-1}^{(i)}, u_k) \\ &\quad - \sum_{i=0}^{2n} W_i^{(m)} \hat{x}_k^{(i)})(\sum_{j=1}^{k} K_j \hat{x}_{k-j}^+)^T + \sum_{j=1}^{k} K_j \hat{x}_{k-j}^+ (\hat{x}_{k-j}^+)^T (K_j)^T + Q_k \end{aligned}$$

According to Equation (12), we substitute $f(\hat{x}_{k-1}^{(i)}, u_k)$ with $\hat{x}_k^{(i)}$ in the equation and expand the expectation in the equation, substitute $E()$ with $\sum_{i=0}^{2n} W_i^{(c)}$, thus, the covariance matrix can finally be displayed as:

$$\begin{aligned} P_k^- = & \sum_{i=0}^{2n} W_i^{(c)} (\hat{x}_k^{(i)} - \sum_{i=0}^{2n} W_i^{(m)} \hat{x}_k^{(i)})(\hat{x}_k^{(i)} - \sum_{i=0}^{2n} W_i^{(m)} \hat{x}_k^{(i)})^T \\ & + \sum_{i=1}^{k} (K_j x_{k-j} \sum_{i=0}^{2n} W_i^{(c)} (\hat{x}_k^{(i)} - \sum_{i=0}^{2n} W_i^{(m)} \hat{x}_k^{(i)})^T) \\ & + \sum_{i=1}^{k} \sum_{i=0}^{2n} W_i^{(c)} (\hat{x}_k^{(i)} - \sum_{i=0}^{2n} W_i^{(m)} \hat{x}_k^{(i)})(\hat{x}_{k-j}^{+})^T (K_j)^T \\ & + \sum_{j=1}^{k} K_j \hat{x}_{k-j}^{+} (\hat{x}_{k-j}^{+})^T (K_j)^T + Q_k \end{aligned} \tag{15}$$

Step 5: Transform the sigma points to the measurement estimation points:

$$\hat{y}_k^{(i)} = h(\hat{x}_k^{(i)}, u_k) \tag{16}$$

Step 6: Calculate the mean and the covariance matrix of the measurement estimation:

$$\hat{y}_k = \sum_{i=0}^{2n} W_i^{(m)} \hat{y}_k^{(i)} \tag{17}$$

and the covariance matrix of the measurement estimation is:

$$P_y = \sum_{i=0}^{2n} W_i^{(c)} (\hat{y}_k^{(i)} - \hat{y}_k)(\hat{y}_k^{(i)} - \hat{y}_k)^T + R_k \tag{18}$$

Step 7: Calculate the covariance between $\hat{x}_k^-$ and $\hat{y}_k$:

$$P_{xy} = \sum_{i=0}^{2n} W_i^{(c)} (\hat{x}_k^{(i)} - \hat{x}_k)(\hat{y}_k^{(i)} - \hat{y}_k)^T \tag{19}$$

Step 8: The process of the state measurement update is:

$$\begin{aligned} K_k &= P_{xy} P_y^{-1} \\ \hat{x}_k^+ &= \hat{x}_k^- + K_k (y_k - \hat{y}_k) \\ P_k^+ &= P_k^- - K_k P_y K_k^T \end{aligned} \tag{20}$$

4. Model Parameter Identification

The accuracy of SOC estimation depends heavily on the estimation accuracy of the battery capacity and precise model parameters. The battery parameters R_0, R_1, C_1, R_2, C_2, α and β shown in Equation (7) are related to *SOC* value. The battery parameters cannot be measured directly. Thus, the unknown parameters are to be identified and calculated in this section to acquire the equivalent circuit information.

4.1. Test Bench

A test bench is established to verify the effectiveness of the proposed method. The test bench is taken under the temperature at 25 ± 2 °C and by the laboratory equipments of the BTS-4000 battery testing system(BTS-4000-6V4A-CCDC-USB, NEWARE Electronic Co., Ltd, Shenzhen, China), which have a measurement current range of 0–3000 A and voltage range of 0–110 V and temperature range of −25–100 °C with the sampling period 100 ms. Moreover, the *SOC* value can be obtained through the Ah counting by the software after configuring some test profiles and parameters. The test object is a ternary manganese-nickel-cobalt (MNC) lithium battery (Sony Corporation, Tokyo, Japan) pack shown in the red oval coil of Figure 2, which consists of ten Sony commercial cells (US18650GR G7, Sony Corporation, Tokyo, Japan) in parallels and has a nominal capacity of 24 Ah, a nominal voltage of 3.7 V, a charging cut-off voltage of 4.2 V and a discharging cut-off voltage of 3.0 V. Some prior discussions are provided firstly as followings:

1. When the battery capacity is measured with 1 C, 2 C and 3 C discharge rates. The corresponding results are 23.587 Ah, 23.294 Ah and 22.460 Ah, respectively. It is shown that the discharge capacity at higher rates is lower than that at low rates and it is different from the nominal value 24 Ah. For the non-fresh lithium battery pack, it is acceptable that the discharge capacity is slightly less than 24 Ah of the nominal capacity. Hence, the rated capacity of the battery is considered as 23.587 Ah instead of 24 Ah.
2. Since the measurement error of the current and voltage of the test platform is less than 0.1% of full scale, it is feasible to assume that the battery *SOC* value can be obtained by this high-precision battery testing system BTS-4000. Hence, the obtained *SOC* is used as a true *SOC* value although some sensor errors exist.
3. For convenience, the integer order model can be obtained by setting the orders of the fractional capacitors $\alpha = \beta = 1$. The physical meanings of all the seven parameters of the battery second-order RC model are identical no matter whether the model is a fractional order model or an integer order model.

A universal method to identify the battery model parameter is the battery pulse characterization experiment. A pulse characterization experiment which is derived from discharging and standing process is intended, and it is shown as Figure 3. With the voltage and current curves of the pulse characterization experiment, the seven unknown parameters can be determined and this is the previous work of the battery SOC estimation with FUKF.

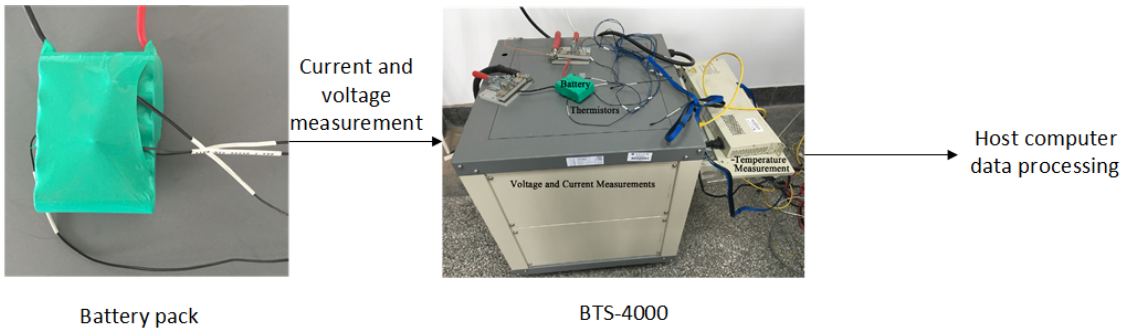

Figure 2. Test bench and battery.

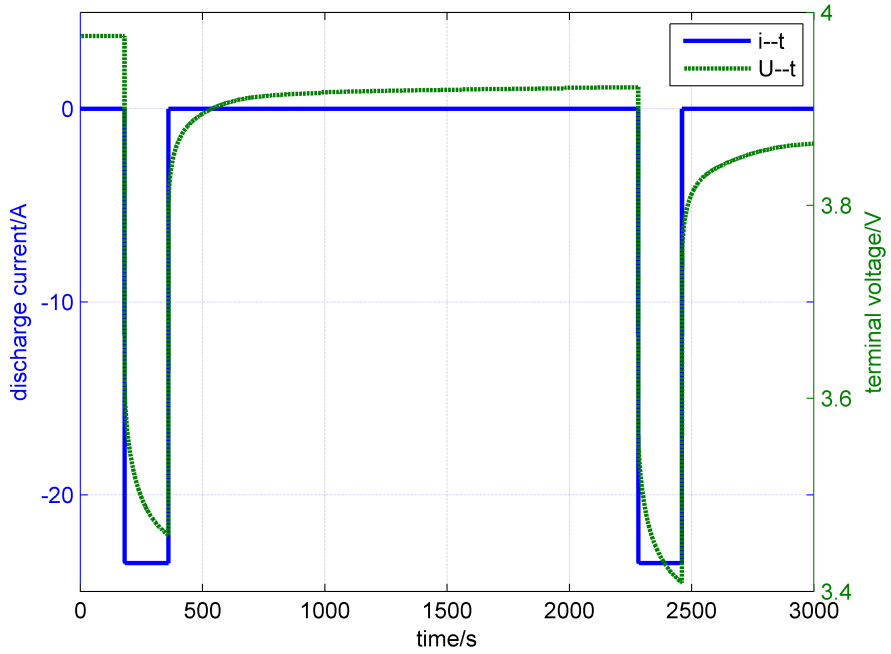

Figure 3. The part of the pulse characterization profile.

4.2. The Identification for Resistor R_0

The instantaneous voltage drop at the beginning of the discharging process is caused by the resistor R_0. The terminal voltage before the current discharge pulse appears is considered as the battery electrodynamic force, E, because the voltages of the capacitors C_1 and C_2 can be considered to 0 V. Thus, with the terminal voltage U at the beginning of the discharging process, the resistor can be determined as:

$$R_0 = \frac{E - U}{I} \tag{21}$$

4.3. RC Loop Identification

The responses of the two RC loops in Figure 1 are as:

$$\begin{aligned} U_1(t) &= U_1(t_0)e^{-\frac{t-t_0}{\tau_1}} + IR_1(1 - e^{-\frac{t-t_0}{\tau_1}}) \\ U_2(t) &= U_2(t_0)e^{-\frac{t-t_0}{\tau_2}} + IR_2(1 - e^{-\frac{t-t_0}{\tau_2}}) \end{aligned} \tag{22}$$

The response consists of the zero-input response and the zero-state response, and the parameters $\tau_1 = R_1C_1$ and $\tau_2 = R_2C_2$ are the time constants of the two RC loops. These two time constants represent the rate of convergency of the terminal voltage curve at the discharge process and standing process.

At the discharging process, $U_1(t_0)$ and $U_2(t_0)$ equal zero, and according to the model voltage in Equation (1), the battery voltage are:

$$U_i(t) = E(SOC) - IR_1(1 - e^{-\frac{t-t_0}{\tau_1}}) - IR_2(1 - e^{-\frac{t-t_0}{\tau_2}}), \tag{23}$$

thus the least square method [36] is used to fit the terminal voltage $U(t)$ of discharging process curve. With the exponential fitting, the time constants τ_1 and τ_2 can be determined. At t_f, which is the time of the end of the discharging process, $U_1(t_f)$ and $U_2(t_f)$ can be determined, thus, R_1, R_2, C_1, C_2 can all be identified.

Then considering the voltage $U_1(t)$ and $U_2(t)$ with the fractional order α and β, and integrating Equation (5), this derives:

$$\begin{aligned} U_{f1}(t) &= h^{\alpha} \sum_{j=0}^{k} w_j^{-\alpha} \frac{R_1 I(t-jh) - U_1(t-jh)}{R_1 C_1} \\ U_{f2}(t) &= h^{\beta} \sum_{j=0}^{k} w_j^{-\beta} \frac{R_2 I(t-jh) - U_2(t-jh)}{R_2 C_2} \end{aligned} \tag{24}$$

According to Equation (5), the battery terminal voltage in fractional form at the standing process can be derived as:

$$\begin{aligned} U_f(t) =& E(SOC) - U_{f1}(t) - U_{f2}(t) - IR_0 \\ =& E(SOC) - h^{\alpha} \sum_{j=0}^{k} w_j^{-\alpha} \frac{R_1 I(t-jh) - U_1(t-jh)}{R_1 C_1} \\ & - h^{\beta} \sum_{j=0}^{k} w_j^{-\beta} \frac{R_2 I(t-jh) - U_2(t-jh)}{R_2 C_2} \end{aligned} \tag{25}$$

and also the least square method is used to find a group of values of α and β. The values aim to minimize the error between $U_i(t)$ and $U_f(t)$ with the performance indicator [26]:

$$J = min \int_0^{+\infty} ||U_f(t) - U_i(t)||^2 dt. \tag{26}$$

5. Experimental Verification

To illustrate the effectiveness of fractional second-order RC model and FUKF, three experiments are developed on the battery test bench for the MNC lithium battery pack. The three experiments are pulse characterization experiment, static discharge experiment and dynamic discharge experiment, respectively. Pulse characterization experiment is performed for the parameter identification of the battery model, and static discharge experiment and dynamic discharge experiment are performed to validate the proposed SOC estimation method based on FUKF. These two experiments are operated with a discharge current rate of 1C and the dynamic pulse condition, respectively.

5.1. Pulse Characterization Experiment

A pulse characterization experiment such as in Figure 3 is developed to identify the battery model parameters. The battery initial *SOC* is set to 100%. The current of the discharging process is set to 1 C. The discharging time is set to 180 s to bring the battery *SOC* with a 0.05 reduction. The standing process time after the discharging process is set to be 1500 s. According to Equations (21)–(23), R_0, R_1, C_1, R_2, C_2 can be identified. The results of the parameter identification are shown as Figure 4. The capacitances and resistances in the model are treated as identical for both the integer and fractional models, because the difference of the integer and fractional model is the orders of the capacitors according to the definition of the fractional capacitor model. According to Equation (24), the orders of C_1 and C_2 are determined by minimizing the performance indicator in Equation (26). From Figure 4, the battery model parameters vary with the value of *SOC*. When the *SOC* value decreases from 1 to 0, the resistances of the battery model including R_0, R_1 and R_2 fluctuate slightly. However, the capacitances of the battery model including C_1 and C_2 ascend first and then descend and the peak values appear when *SOC* value is 0.6. This phenomenon is caused by the battery polarization effect and the capacitors of the second-order RC model successfully explains the effect. When the *SOC* value is less than 0.2, the battery dynamic becomes different, thus the parameters, especially R_1 and R_2 fluctuate steeply. The orders of the two capacitors, α and β, hint a bigger time constant, thus the second-order model can

depict a more obvious polarization effect with the fractional order calculus. In addition, the results of the orders α and β of capacitors C_1 and C_2 are given as Figure 5. The parameter identification is developed by the discharging process curve, thus the orders remain constant within a circle of the discharging process. From Figure 5, the order of C_1 is larger than 1 mostly. Radwan et al. have pointed out that fractional capacitors whose order is larger than 1 are still fractional capacitors and C_1 can be regarded as a fractional capacitor whose order is less than 1 in series with an integer capacitor [37].

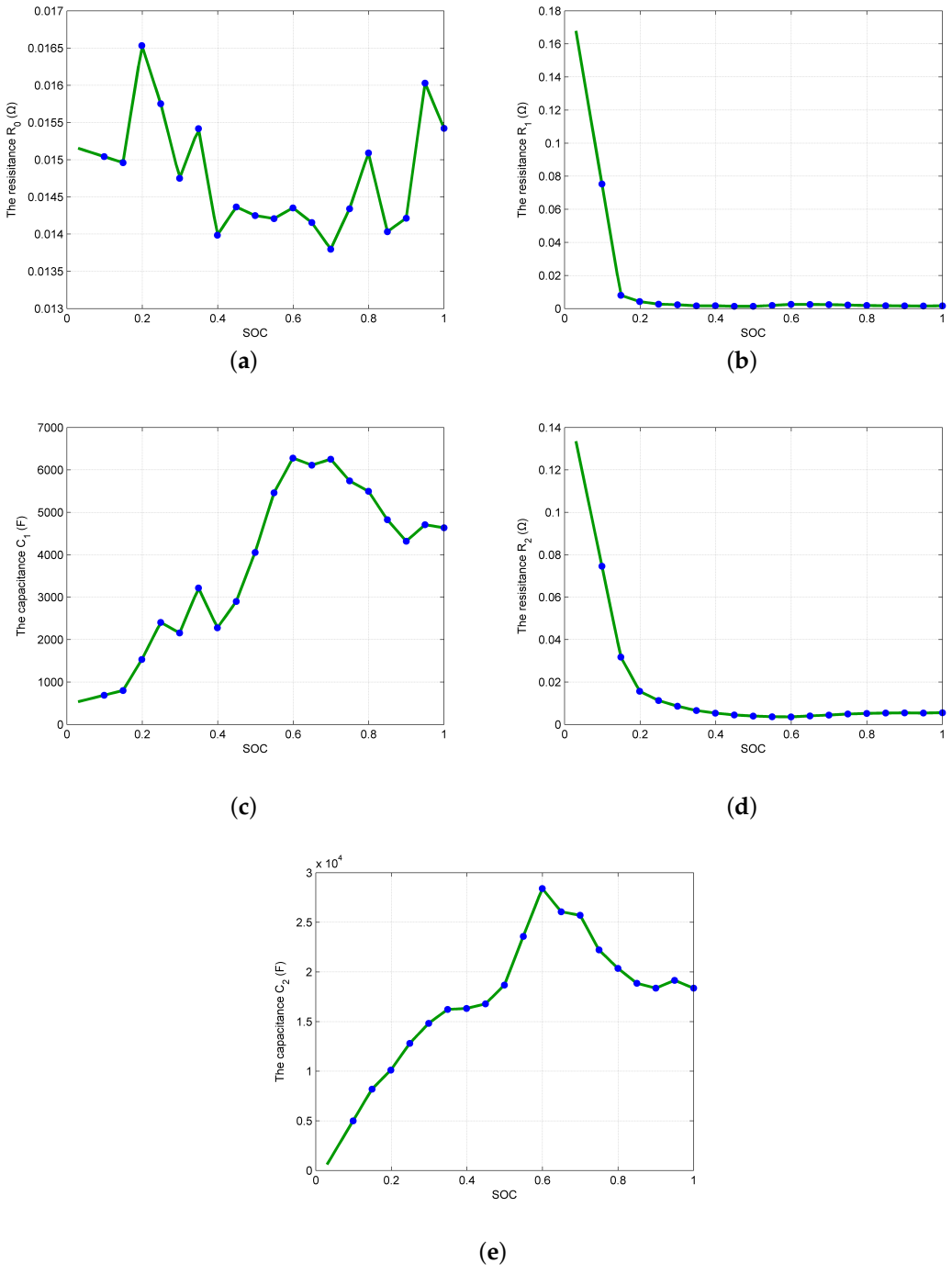

Figure 4. The results of parameter identification. (**a**) The curve of R_0 with respect to SOC; (**b**) The curve of R_1 with respect to SOC; (**c**) The curve of C_1 with respect to SOC; (**d**) The curve of R_2 with respect to SOC; (**e**) The curve of C_2 with respect to SOC.

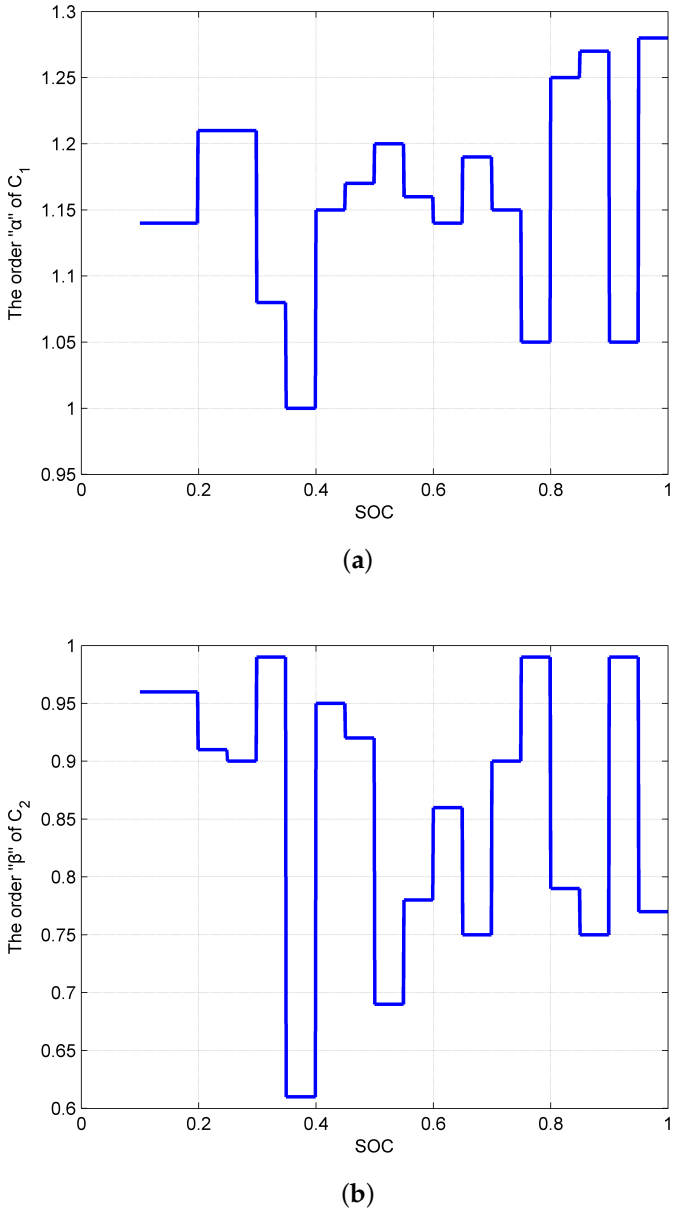

Figure 5. The orders of the capacitors. (**a**) The order α of C_1 with respect to SOC; (**b**) The order β of C_2 with respect to SOC.

5.2. Static Discharge Experiment

To prove the static characteristic of the battery model and FUKF, the static experiment with a discharge current rate of 1 C is adopted. The static experimental validation current profile is shown as Figure 6.

To validate the convergent properties of FUKF and UKF, it is assumed that the initial *SOC* value is unknown, thus the estimation values of initial *SOC* are both set to 0.9 intentionally while the actual *SOC* value is 1.0, which means an initial *SOC* value error exists. The results under static discharge experiment are given as Figure 7. From Figure 7, the static discharge experiment result comparison of FUKF and UKF is shown as Table 1.

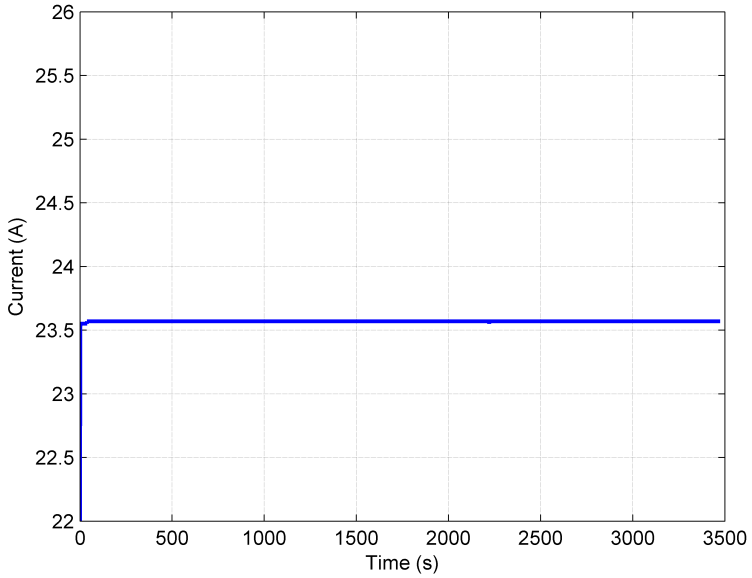

Figure 6. Static experimental validation current profile.

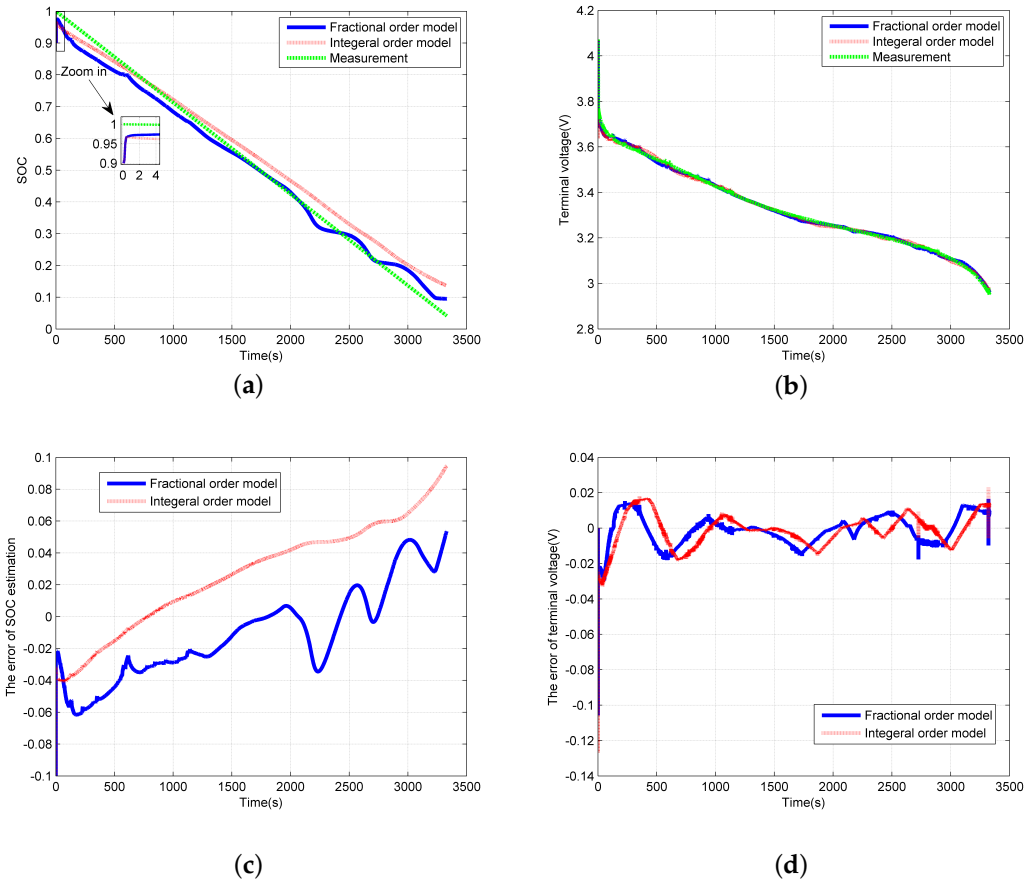

Figure 7. The results of static discharge experiment. (**a**) The results of SOC estimation; (**b**) The results of battery terminal voltage estimation; (**c**) The errors of SOC estimation; (**d**) The errors of battery terminal voltage estimation.

Table 1. Static discharge experiment result comparison.

Method	SOC Error		Maximum Terminal Voltage Error
	Maximum Error	Mean Error	
FUKF	5.36%	2.56%	0.0296 V
UKF	9.47%	3.65%	0.0328 V

In static discharging experiment, the fractional second-order RC model and FUKF algorithm show a more accurate performance on the estimation of battery SOC and battery terminal voltage, where the SOC error and the battery terminal voltage error are 5.36% bound and 0.0296 V bound, respectively. However, the SOC error and the battery terminal voltage error of the integer model and UKF are 9.47% bound and 0.0328 V bound, respectively. In real system, to illustrate the robustness and stability of SOC estimation for most of the working time, mean error is utilized as an indicator instead of maximum estimation error. Thus, the mean errors of SOC estimation of FUKF algorithm and UKF algorithm are given as 2.56% and 3.65%, respectively.

5.3. Dynamic Discharge Experiment

To verify the dynamic characteristic of the battery model and FUKF, the dynamic pulse condition is adopted. The magnitude of the current profile is scaled to obtain the voltage response with respect to the whole SOC range. The current profile of dynamic experimental validation is shown as Figure 8. The results under dynamic discharge experiment are given as Figure 9. The dynamic discharge experiment result comparison of FUKF and UKF is shown as Table 2.

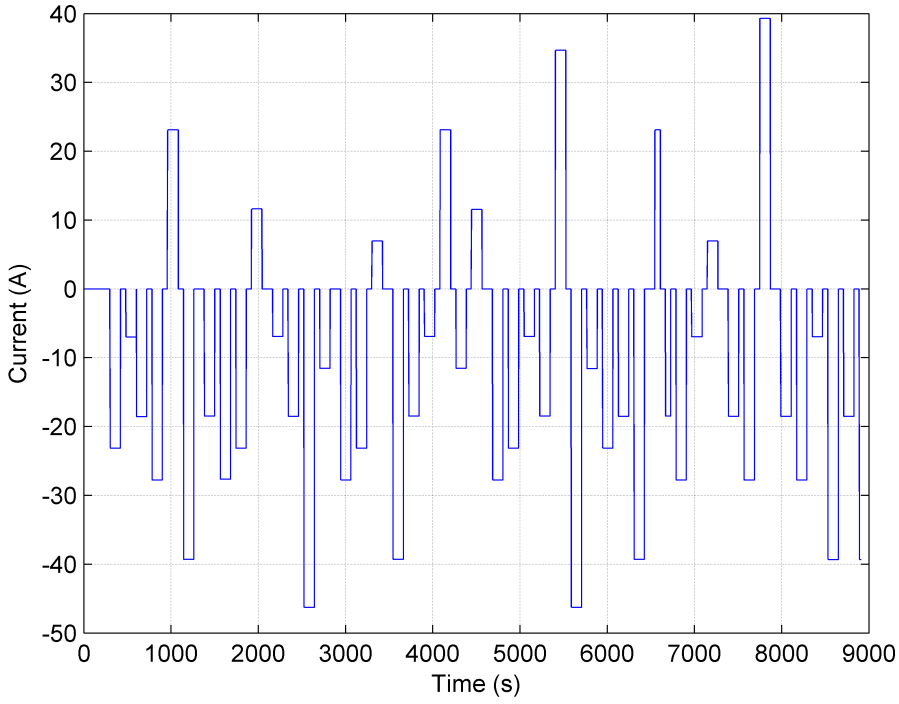

Figure 8. The current profile of dynamic experimental validation.

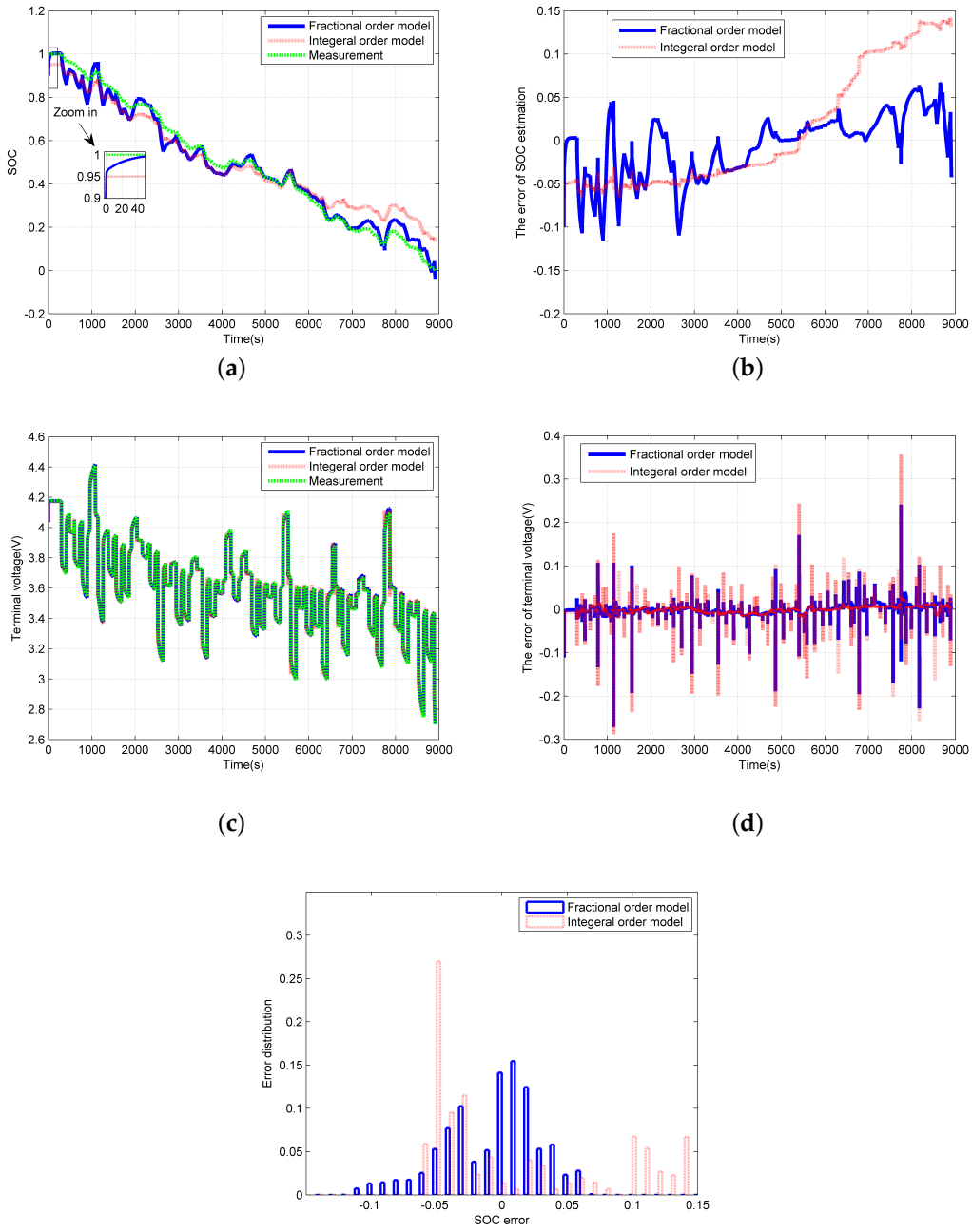

Figure 9. The results of dynamic discharge experiment. (**a**) The results of SOC estimation; (**b**) The errors of SOC estimation; (**c**) The results of battery terminal voltage estimation; (**d**) The errors of battery terminal voltage estimation; (**e**) The distribution of the estimation error.

Table 2. Dynamic discharge experiment result comparison.

Method	SOC Error		Maximum Terminal Voltage Error
	Maximum Error	Mean Error	
FUKF	11.55%	2.88%	0.2712 V
UKF	14.20%	5.92%	0.3568 V

With Figure 9, there are some results as:

1. The fractional second-order RC model and FUKF algorithm track the measured SOC and terminal voltage well. The SOC error and the battery terminal voltage error are 11.55% bound and 0.2712 V bound, respectively. On the contrast, the SOC error and the battery terminal voltage error of the integer model and UKF are 14.20% bound and 0.3568 V bound, respectively. The mean errors of SOC estimation based on FUKF algorithm and UKF algorithm are also given as 2.88% and 5.92%, respectively. Although the maximal error of the SOC estimation based on FUKF algorithm is quite large, the mean error is mild enough. Thus, for most time, FUKF algorithm presents extraordinary precision on SOC estimation.
2. In both static and dynamic experiments, the result curves of fractional order model and integer order model can both converge to the measurement curve even though the initial *SOC* values are incorrect and the curve of fractional order model recovers the initial SOC error on a larger scale and with less time according to the enlarged drawings. This demonstrates better stability and robustness of FUKF.
3. In both static and dynamic discharge experiment, both UKF and FUKF show a convergent performance. However, when the remaining capacity of the battery is little, due to the enlarged battery polarization effect, the battery model parameter estimation becomes inaccurate. This leads to the error of the space state estimation. UKF loses its convergence and performs divergently. Nevertheless, the fractional second-order RC model and FUKF algorithm could still make precise estimation of the battery parameters and track the actual value of *SOC*.
4. Compared with the integer model, the fractional orders of the capacitors C_1 and C_2 are more capable of reducing the performance indicator in Equation (26) with least square method, because the fractional order model and fractional parameter identification reflect the system performance more precisely.
5. It is obvious that some sharp peaks of the terminal voltage error appear at the beginning and the end of the discharge process in Figure 9d. That is because the battery model parameters suddenly change at the instant the battery current pulse appears or disappears. This phenomenon is caused by the battery polarization effect. The fractional order model and FUKF exhibit a more accurate performance on the suppression of sharp peak error. In dynamic operation condition, the error of the terminal voltage estimation is more severe than in the static operation condition, because the battery polarization effect is more obvious in the rapidly changing operating conditions. This effect causes the dynamics which cannot be modeled. However, FUKF is still effective with this phenomenon.

The characteristics of the battery can be described by the fractional order model more accurately. FUKF algorithm can effectively guarantee the state estimation accuracy. The precision of the c estimation can be improved significantly by combing the fractional model and FUKF algorithm. The proposed method performs accurately and reliably on terminal voltage and SOC estimation in complicated working condition. The proposed method can be applied in real BMS.

6. Conclusions

In this paper, a fractional second-order RC circuit model is presented, and an algorithm combining UKF and fractional calculus is proposed to estimate the battery SOC. The algorithm can be easily implemented and applied by iteration, and it is suitable for the SOC estimation of electric vehicle BMS. The algorithm, FUKF, has been proved to guarantee the performance of the SOC estimation. The fractional battery model and FUKF fit the dynamic characteristics precisely. Their behavior of battery parameter identification is better than the integer one. These properties explain the precision of SOC estimation and terminal voltage estimation of FUKF. The experimental results show robustness on suppressing the noise and disturbance caused by the inexact or unknown statistical properties of the system modeling error and measurement error.

Acknowledgments: This work was supported by the National Natural Science Foundation of China (No. 61640310 and 61773323).

Author Contributions: Yixing Chen and Deqing Huang planned the intial aide and designed the algorithm under the literature review. Yixing Chen and Deqing Huang wrote the original manuscript. Qiao Zhu and Weiqun Liu established the experiment bench. Qiao Zhu, Weiqun Liu and Cong zhi and Neng Xiong analyzed the experimental date. Yixing Chen, Congzhi Liu and Neng Xiong revised the finsl manuscript.

Conflicts of Interest: The authors declare no conflicts of interest.

References

1. Qiu, S.; Chen, Z.; Masrur, M.A.; Murphey, Y.L. Battery hysteresis modeling for state of charge estimation based on Extended Kalman Filter. In Proceedings of the 2011 6th IEEE Conference on Industrial Electronics and Applications (ICIEA), Beijing, China, 21–23 June 2011; pp. 184–189.
2. Li, J.; Lai, Q.; Wang, L.; Lyu, C.; Wang, H. A method for SOC estimation based on simplified mechanistic model for $LiFePO_4$ battery. *Energy* **2016**, *114*, 1266–1276.
3. Ma, Y.; Zhou, X.; Li, B.; Chen, H. Fractional modeling and SOC estimation of lithium-ion battery. *IEEE/CAA J. Autom. Sin.* **2016**, *3*, 281–287.
4. Doucette, R.T.; McCulloch, M.D. Modeling the prospects of plug-in hybrid electric vehicles to reduce CO_2 emissions. *Appl. Energy* **2011**, *88*, 2315–2323.
5. He, H.; Xiong, R.; Guo, H. Online estimation of model parameters and state-of-charge of $LiFePO_4$ batteries in electric vehicles. *Appl. Energy* **2012**, *89*, 413–420.
6. Aylor, J.H.; Thieme, A.; Johnso, B.W. A battery state-of-charge indicator for electric wheelchairs. *IEEE Trans. Ind. Electron.* **1992**, *39*, 398–409.
7. Plett, G.L. Extended Kalman filtering for battery management systems of LiPB-based HEV battery packs: Part 3. State and parameter estimation. *J. Power Sources* **2004**, *134*, 277–292.
8. Zhang, F.; Liu, G.J.; Fang, L.J.; Wang, H.G. Estimation of Battery State of Charge With H-infinity Observer: Applied to a Robot for Inspecting Power Transmission Lines. *IEEE Trans. Ind. Electron.* **2012**, *59*, 1086–1095.
9. Belhani, A.; M'Sirdi, N.K.; Naamane, A. Adaptive Sliding Mode Observer for Estimation of State of Charge. *Energy Procedia* **2013**, *42*, 377–386.
10. Xia, B.; Chen, C.; Tian, Y.; Wang, M.; Sun, W.; Xu, Z. State of charge estimation of lithium-ion batteries based on an improved parameter identification method. *Energy* **2015**, *90*, 1426–1434.
11. Dai, H.; Guo, P.; Wei, X.; Sun, Z.; Wang, J. ANFIS (adaptive neuro-fuzzy inference system) based online SOC (State of Charge) correction considering cell divergence for the EV (electric vehicle) traction batteries. *Energy* **2015**, *80*, 350–360.
12. Yao, L.W.; Aziz, J.A.; Idris, N.R.N. State-of-charge estimation for lithium-ion battery using Busse's adaptive unscented Kalman filter. In Proceedings of the 2015 IEEE Conference onEnergy Conversion (CENCON), Johor Bahru, Malaysia, 19–20 October 2015; pp. 227–232.
13. Sun, F.; Hu, X.; Zou, Y.; Li, S. Adaptive unscented Kalman filtering for state of charge estimation of a lithium-ion battery for electric vehicles. *Energy* **2011**, *36*, 3531–3540.
14. Julier, S.J.; Uhlmann, J.K. New extension of the Kalman filter to nonlinear systems. In Proceedings of the International Society for Optics and Photonics, Orlando, FL, USA, 21–25 April 1997; pp. 182–193.
15. Plett, G.L. Sigma-point Kalman filtering for battery management systems of LiPB-based HEV battery packs: Part 1: Introduction and state estimation. *J. Power Sources* **2006**, *161*, 1356–1368.
16. Plett, G.L. Sigma-point Kalman filtering for battery management systems of LiPB-based HEV battery packs: Part 2: Simultaneous state and parameter estimation. *J. Power Sources* **2006**, *161*, 1369–1384.
17. Tian, Y.; Xia, B.; Sun, W.; Xu, Z.; Zheng, W. A modified model based state of charge estimation of power lithium-ion batteries using unscented Kalman filter. *J. Power Sources*, **2014**, *270*, 619–626.
18. D'Alfonso, L.; Lucia, W.; Muraca, P.; Pugliese, P. Mobile robot localization via EKF and UKF: A comparison based on real data. *Robot. Auton. Syst.* **2015**, *74*, 122–127.
19. Miyabayashi, K.; Tonomura, O.; Kano, M.; Hasebe, S. Comparative study of state estimation of tubular microreactors using ukf and ekf. *IFAC Proc. Vol.* **2012**, *45*, 513–518.
20. He, Z.; Chen, D.; Pan, C.; Chen, L.; Wang, S. State of charge estimation of power Li-ion batteries using a hybrid estimation algorithm based on UKF. *Electrochim. Acta* **2016**, *211*, 101–109.

21. Monje, C.A.; Chen, Y.Q.; Vinagre, B.M.; Xue, D.; Feliu-Batlle, V. *Fractional-Order Systems and Controls: Fundamentals and Applications*; Springer Science & Business Media: Berlin, Germany, 2010.
22. Podlubny, I. *Fractional Differential Equations: An Introduction to Fractional Derivatives, Fractional Differential Equations, to Methods of Their Solution and Some of Their Applications*; Academic Press: Cambridge, MA, USA, 1998.
23. Ortigueira, M.D.; Machado, J.A.T. Fractional calculus applications in signals and systems. *Signal Process.* **2006**, *86*, 2503–2504.
24. Petras, I. *Fractional-Order Nonlinear Systems: Modeling, Analysis and Simulation*; Springer Science & Business Media: Berlin, Germany, 2011.
25. Zhang, L.; Hu, X.; Wang, Z.; Sun, F.; Dorrell, D.G. Fractional-order modeling and State-of-Charge estimation for ultracapacitors. *J. Power Sources* **2016**, *314*, 28–34.
26. Liu, C.; Liu, W.; Wang, L.; Hu, G.; Ma, L.; Ren, B. A new method of modeling and state of charge estimation of the battery. *J. Power Sources* **2016**, *320*, 1–12.
27. Hu, X.; Li, S.; Peng, H. A comparative study of equivalent circuit models for Li-ion batteries. *J. Power Sources* **2012**, *198*, 359–367.
28. Hu, Y.; Yurkovich, S.; Guezennec, Y.; Guezennec, Y. Electro-thermal battery model identification for automotive applications. *J. Power Sources* **2011**, *196*, 449–457.
29. Westerlund, S.; Ekstam, L. Capacitor theory. *IEEE Trans. Dielectr. Electr. Insul.* **1994**, *1*, 826–839.
30. Ng, K.S.; Moo, C.S.; Chen, Y.P.; Hsieh, Y.C. Enhanced coulomb counting method for estimating state-of-charge and state-of-health of lithium-ion batteries. *Appl. Energy* **2009**, *86*, 1506–1511.
31. Caponetto, R. *Fractional Order Systems: Modeling and Control Applications*; World Scientific: Singapore, 2010.
32. Simon, D. *Optimal State Estimation: Kalman, H Infinity, and Nonlinear Approaches*; John Wiley & Sons: Hoboken, NJ, USA, 2006.
33. Park, S. Fixed point theorems for better admissible multimaps on almost convex sets. *J. Math. Anal. Appl.* **2007**, *329*, 690–702.
34. Nosrati, K.; Rostami, A.S.; Azemi, A.; Pariz, N. Unscented Kalman Filter Applied to noisy synchronization of Rossler chaotic system. In Proceedings of the 2011 3rd International Conference on Advanced Computer Control (ICACC), Harbin, China, 18–20 January 2011; pp. 378–383.
35. Haykin, S. *Kalman Filtering and Neural Networks*; Wiley: New York, NY, USA, 2001.
36. Unterrieder, C.; Zhang, C.; Lunglmayr, M.; Priewasser, R.; Marsili, S.; Huemer, M. Battery state-of-charge estimation using approximate least squares. *J. Power Sources* **2015**, *278*, 274–286.
37. Radwan, A.G.; Elwakil, A.S.; Soliman, A.M. On the generalization of second-order filters to the fractional-order domain. *J. Circuits Syst. Comput.* **2009**, *18*, 361–386.

© 2017 by the authors. Licensee MDPI, Basel, Switzerland. This article is an open access article distributed under the terms and conditions of the Creative Commons Attribution (CC BY) license (http://creativecommons.org/licenses/by/4.0/).